International Journal of Impact Engineering, Volume 80, June 2015, pp. 152-161
DOI:10.1016/j.ijimpeng.2015.02.010

Gas gun ramp loading of Kel-F 81 targets using a ceramic graded areal density flyer system

M Goff[1,2], P J Hazell[3], G J Appleby-Thomas[2], D C Wood[2], C Stennett[2] and P Taylor[1]

[1]AWE, Aldermaston, Reading, RG7 4PR, UK

[2]Centre for Defence Engineering, Cranfield University, Defence Academy of the United Kingdom, Shrivenham, SN6 8LA

[3] School of Engineering and Information Technology, UNSW Canberra, The University of New South Wales, Northcott Drive, Canberra, ACT 2600, Australia

Email: m.goff@cranfield.ac.uk

Abstract. Kel-F 81 (PCTFE / Polychlorotrifluoroethylene) polymer targets were subjected to ramp loadings generated by a ceramic flyer accelerated into the targets by a gas gun in the plate impact configuration. This approach used a ceramic graded areal density flyer in conjunction with a ceramic buffer plate to induce a ramp loading in the target. The flyer was comprised of a rapid prototyped alumina ceramic. The loading was observed with embedded electromagnetic particle velocity gauges (PV gauges) with the results

compared with ANSYS Autodyn™ hydrocode simulations. Experimental results show that ramp loadings of varying duration and magnitude were induced into the target. These loadings can be described as shockless compressions leading to shocked states within the material. In addition, numerical simulations provided further insight into the loading approach – with good agreement found with experimental data, opening the potential to design more complex loading systems in future.

Keywords: Ramp Wave, Ceramic, Gas Gun, Graded Areal Density, Hydrocode Modelling

1. Introduction

This paper details the development of a ramp loading technique that can be used to impart controlled ramp loading paths (ideally a ramp leading to a period of sustained shock) in polymer or PBX (Polymer Bonded Explosive) targets. The eventual aim of this body of work is to develop a methodology that can be used to study the effects of ramp loading on run to detonation in explosive targets. This paper details the development and application of this technique with inert polymer targets; initial experiments and work on energetic targets have been reported previously elsewhere [1,2]. Experimental constraints dictated that the technique used had to be compatible with both the gas gun plate impact [3] and embedded particle velocity (PV) gauge techniques [4,5]. This meant that several approaches to generate ramp loadings previously reported in the literature using metallic materials [6,7] were unable to be

employed [8]. Therefore a novel method was developed based on the concept devised by Winter et al. [9] of using a flyer with a graded areal density. Whereas Winter et al. used metallic flyers, this variation on the technique uses flyers comprised of alumina ceramic.

The primary diagnostic used in this work is the embedded particle velocity gauge. The technique used here was a modified version of the methodology developed at LANL [4,5,10,11]. This technique uses a gauge package consisting of multiple metallic elements in conjunction with a known flat magnet field. Careful metrology and alignment combined with Faradays law of induction enable the particle velocity (the velocity of the continuum elements of the target material propagating an induced wave or shock) experienced by the gauge elements to be calculated (from a measured voltage). It is assumed the gauge elements move with the surrounding material and do not significantly disrupt the one dimensional flow of any wave or shock being experienced.

3. Concept

Isentropic or ramp loadings have previously been generated using a variety of technologies. Here, a number of common techniques are examined to provide an overview of the field.

A widespread approach (in conjunction with gas gun/ explosively driven launcher methods) is the use of a solid impactor with a graded density. Some examples of this approach are multiple layers of materials with an increasing density gradient [12] or a fabricated flyer with a smoothly varying density gradient. Graded structures can be fabricated via a variety of routes; e.g. in the latter case gravity sedimentation [7], powder metallurgy [13], metallic powder loaded resins [6], tape casting [14] or sintering [6]. Graded density approaches have

typically employed metallic materials due to the wide density gradient that is available and the resultant maximal impact pressures that the manufactured flyers can access (due to metals high impedance). A recently developed variation on this method is to use flyers with a graded areal density [9]. This is advantageous as the removal of the need for dis-similar material layers enables a much wider range of materials and fabrication processes to be employed. In this case as material of varying areal density (for example, a spiked structure) drives into a target the proportion of material in contact varies with time – something which, when combined with a buffer plate, allows the time-intensity profile of the imparted wave to be controlled. Another approach is to use impactor materials with a negative elastic moduli or Poisson's ratio (auxetic materials) [15,16]; with this class of materials an initial shock disperses into a ramping wave. Finally, a different methodology is offered by the use of magnetic isentropic compression [17], which employs electromagnetic loading (rather than direct impact) to induce compression in targets.

As outlined above, a wide variety of techniques are available to impact ramped loading profiles into targets. However, these are often very-much dependant on the use of metallic materials. The study reported herein aimed to develop a technique that could be used to investigate the effects of ramp loading on run to detonation in explosive targets. This goal required that the ramp loading methodology used be compatible with embedded particle velocity gauges so that run to detonation processes and in-material behaviour could be observed.

Experimental constraints thus dictated that the ramp loading production method selected had to use non-conductive materials; a minimum density requirement was also imposed by the velocity capabilities of the launcher available. This latter requirement – necessitated by the desire to achieve sufficiently high pressures at the limited impact velocities available to initiate a PBX – meant that an insulating ceramic was selected as a candidate material. Unfortunately, metallic projectiles were not suitable as it has previously been shown that they add significant complexity to the interpretation of PV data [8]. Several techniques for producing solid non-metallic flyers with a density gradient exist, for instance spark plasma sintering [18]. However it was felt that these presented a protracted development route given the limited in-house capabilities in this area. Other techniques such as the use of reverse-elastic moduli materials (e.g. fuzed silica) [16] offered a limited parameter space for adjusting ramp parameters. Therefore a variation (ceramic rather than metallic flyers) on the novel graded areal density concept [9] was selected, as this uses flyers that can be produced using industrial rapid prototyping techniques, thus enabling a rapid progression from theoretical design to experimental results. The other main advantage of the graded areal density method is that in theory the gradient and duration of the ramp loading can be arbitrarily controlled by alteration of the spike and buffer parameters.

The graded areal density system comprises of a system consisting of a flyer plate and a matching (material) buffer plate. The flyer plate has a graded areal density, i.e. it has a surface consisting of multiple raised structures. The technique as employed here uses spikes comprised of square pyramids. This shape was chosen because it enables a high packing density of structures and offers a good match to the capabilities of the rapid prototyping

technique. The buffer plate is made of a similar material and is adhered to the front face of the target (see Figure 1). The flyer is then launched at the target as per the standard gas gun plate impact technique. The properties of the wavefront produced in the target were controlled by alternation of the spike and buffer parameters on an iterative basis, supported by hydrocode modelling.

3. Graded Areal Density Flyers

The combination of complex geometry, ceramic material choice (alumina) and limited order quantity provided a fabrication challenge, preventing employment of conventional machining methods. Ceramic laser stereolithography was eventually chosen as the manufacturing route. This offered a balance between quality of fabrication and ease of availability. This technique uses an ultraviolet laser to produce solid parts out of a photocurable resin loaded with ceramic powder, the parts are then sintered to achieve full density. It is worth noting that a multitude of other additive manufacturing techniques also exist (several of which have the potential t allow ceramic graded areal density structures to be produced); for reference, a useful overview can be found in [19].

Flyer fabrication was carried out by Technology Assessment and Transfer, MD USA [20], with the flyers produced having a quoted structural feature resolution of 200 μm with a measured density of 3740-3750 g/m^3 (using a Mettler-Toledo immersion density balance). Initial tests employed buffer discs manufactured using the same technique. However in later experiments the buffer comprised conventionally pressed tiles of a similar density (ALOTEC 98 SB™). These tiles were employed as they offered a superior surface finish and reduced

the cost of the system. It should be noted that the small difference in material properties between the flyer and buffer did not appear to have an appreciable effect on the operation of the system within this study; notably, this reinforces the close match between the rapid prototyped and conventional alumina material properties in the shock regime.

Eight different flyer designs have been tested, these are detailed below in Figure 1 / Table 1, with Figures 2 and 3 providing further details. Figure 1 and Table 1 jointly show the parameter space explored here. Figure 2 illustrates the variation in normalised areal density with height from the projectile base of these systems. In Figure 2 normalised areal density is defined as the area of a horizontal cross-section through a spike divided by the area of the base of the spike (so that the value for the base of the spike is defined as unity). Note that in case viii, the initial step / drop in density arises due to the requirement to take into account the separation between the base of the spikes. It can be observed that the variation in areal density with position – e.g. the areal density gradient – becomes 'shallower' as the spike height is increased. Further, it should be noted that some as-manufactured flyers used displayed minor defects such as small numbers of truncated spikes; an example of which is highlighted in Figure 3. It is not believed that these anomalies had a significant effect on the experimental results due to the small size of the defect. In addition, at a finer scale, as shown in the micrographs presented in Figure 4, there were also inevitably some systemic aberrations in the tips of the spikes caused by the manufacturing process.

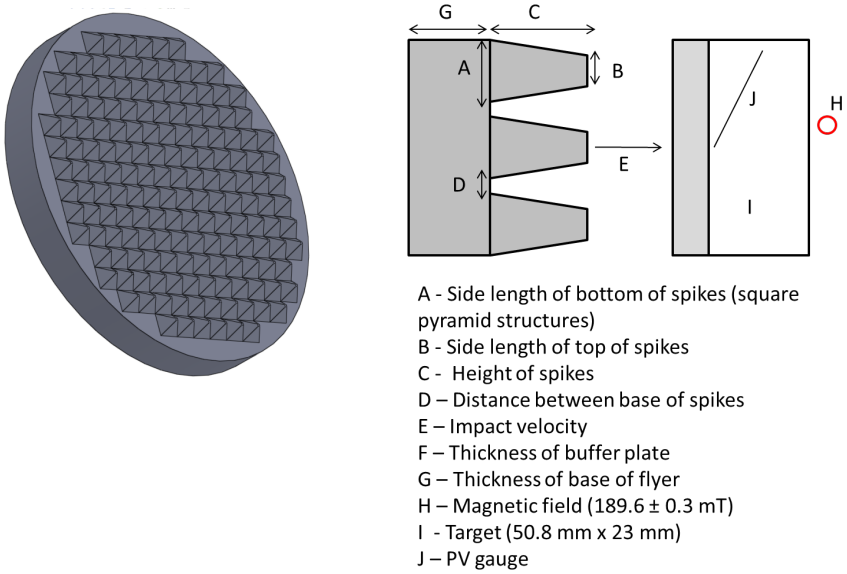

Figure 1: Schematic of 'spiked flyer' with square pyramid spike design. The key variable parameters are shown here and detailed in Table 1.

Flyer	A (mm)	B (mm)	C (mm)	D (mm)	G (mm)
i) 1 mm	3	0.3	1	0	5
ii) 2 mm (variant 1)	3	0.3	2	0	5
iii) 3.5 mm	3	0.3	3.5	0	3.5
iv) 5 mm	3	0.3	5	0	5
v) 10 mm	3	0.3	10	0	5
vi) 2 mm (variant 2)	2	0.3	2	0	5

vii) 2 mm (variant 3)	3	0.3	2	0	10
viii) 2 mm (variant 4)	3	0.3	2	1.5	5

Table 1: Flyer Parameters, letters in top column refer to Figure 1. Buffer thicknesses were either 5 or 4.2 mm.

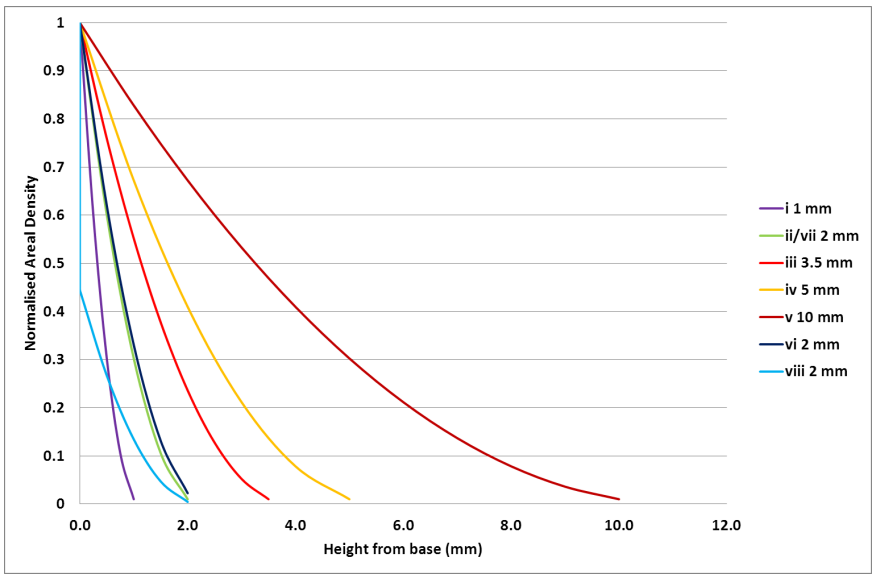

Figure 2: Comparison of calculated normalised areal density for the flyer designs outlined in Table 1.

A) 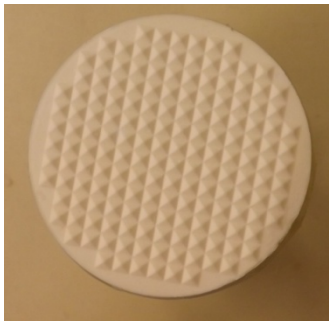 B) 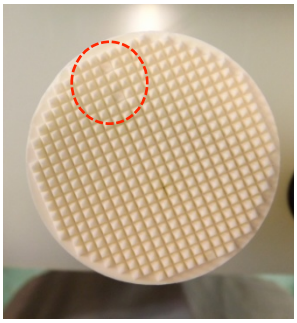 C) 

Figure 3: Images of example flyers A) 1 mm spike height, B) 2 mm spike height with 2 mm base, C) 10 mm spike height. Examples of truncated spikes can be seen in the dashed red circle shown in B).

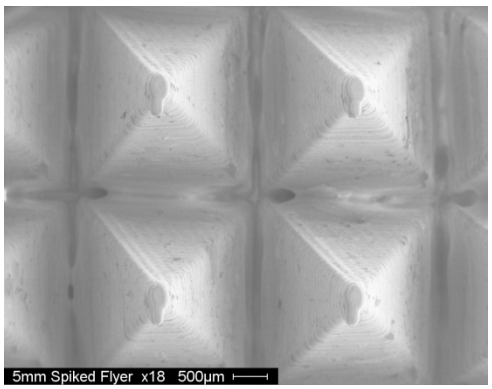

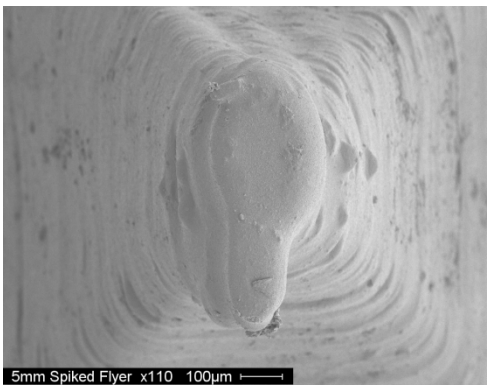

Figure 4: Scanning Electron Microscopy (SEM) images of sections of the 5 mm spike height flyer. The square pyramid spikes are very consistent, albeit with a minor systemic deformation at the tip. The layering in the z-axis (height) is a result of the ceramic stereolithography process.

4. Simulation

In order to try and develop the experimental approach adopted here into a generic approach to ramp wave production, the experimental results were compared to SPH hydrocode simulations created using ANSYS Autodyn™ 14.5 [22]. SPH simulations were used due to the excessive mesh deformation due to material failure. This was so that the consequent timestep issues that would have resulted from the use of a lagrangian mesh were avoided. The use of SPH also avoided the need to introduce an erosion parameter in the simulations that would otherwise be required for lagrangian based simulations. This was important as the results of preliminary lagrangian simulations were found to be sensitive to the erosion parameter used.

The material and particle size parameters used are detailed in Table 2. Due to the complex geometries involved, three-dimensional modelling techniques had to be employed – requiring the generation of a representative geometry. Figure 5 shows the modelled geometry in relation to a full sized target. The simulated geometry represented a portion of the target in the X-Y plane with the Z-axis being the axis of impact. This representation was chosen such that the axis of X-Y symmetry in the model was positioned on the edge of the diagnostic region in the experimental target. Thus if the virtual gauge points at similar z-axis positions in the modelled region record a 1-D wavefront, it can be posited that with regards to the X-Y plane the loading of the gauge elements can be considered one-dimensional. The Z-axis was preserved so that the variation of the loading with depth could be directly compared with experimental results. Due to a lack of a well defined equation of state, strength and failure model for the rapid prototype material and the buffer material, a Johnson-Holmquist model based on a

99.7% pure alumina was used [22]. The density for this material was adjusted slightly to match that of the rapid prototyped material.

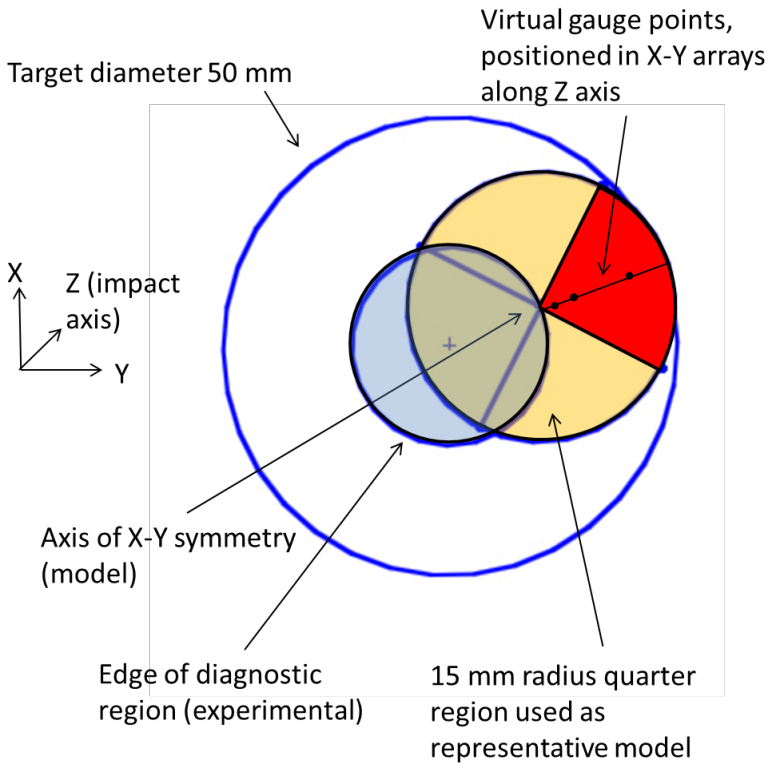

Figure 5: Sketch of representative modelled geometry relation to experimental geometry.

Parameter	Ceramic Flyer	Ceramic Buffer	Kel-F Target
Material model (Shock EoS]	Al 99.7 with modified density [22]	Al 99.7 with modified density	Kel-F [24]
SPH particle size	0.1 mm	0.1 mm	0.2 mm
Strength model	Johnson-Holmquist (JH.)[22,23]	JH.	Von Mises [24,25]
Failure model	JH.	JH.	None

Table 2: Autodyn™ parameters

Figure 6 shows the results from several arrays of virtual gauge points positioned to simulate a finite length particle velocity gauge element. The loading observed is comparable for all virtual gauges in the X-Y plane except those nearest the edge of the representative geometry, an issue likely due to edge release effects that would not be seen in the experimental diagnostic region. This gives confidence that the individual experimental gauge elements are experiencing a loading that can be approximated as one-dimensional for the purposes of PV gauge data analysis (the actual behaviour will strictly speaking be quasi one-dimensional over the gauged region of the target during experimental timescales). The loading can be seen to vary with depth; this is discussed in the following section.

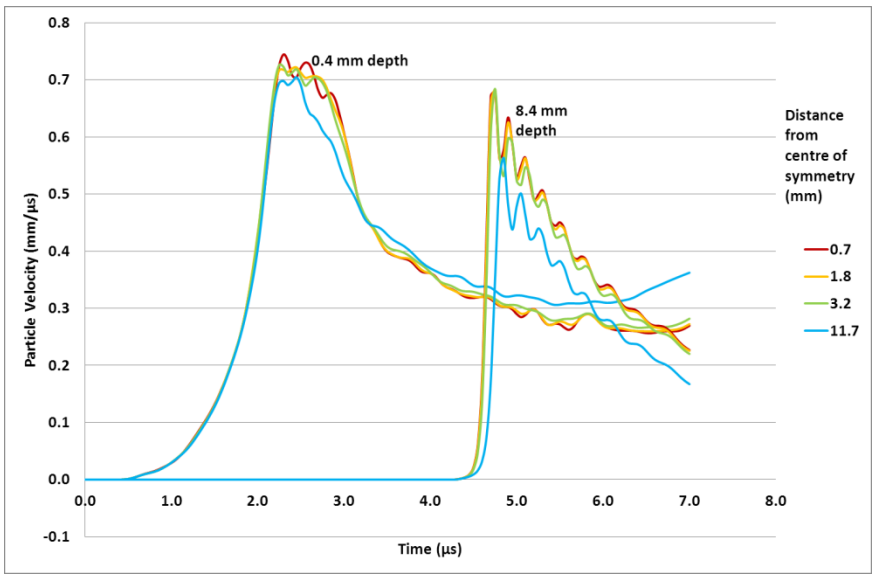

Figure 6: Comparison of particle velocity records for virtual gauge points at multiple positions in Kel-F target for Autodyn™ simulation. 2 mm spike system, 5 mm buffer at 0.95 mm/μs impact velocity.

One area of experimental technique that must be raised is the reaction of a PV gauge element to a pseudo one dimensional wavefront and the consequent potential for discrepancies between true and experimentally measured particle velocity. There are several potential sources of error here. Firstly, if the gauge element is moving in a vector that is not completely perpendicular to the magnetic field, then only the portion of the motion that is perpendicular will be recorded (see equation 1). Secondly, if the wavefront is not planar along the length of the gauge then different parts of the element will be moving at different velocities. Simplistically it may be assumed that the gauge element will record a voltage based upon the averaged velocity across its length. However the true case is likely to be more complex due

to parts of the gauge being at different angles relative to the wavefront. Lastly non 1-D motion could cause spreading of the gauge element, effectively changing its length. This type of motion can be detected experimentally if required, through careful 'misalignment' of the gauge package. However Autodyn™ modelling indicates that the wavefront produced in the target for these experiments is close to one-dimensional (at the resolution of the simulation). To this end, Figure 7 shows the results of a simulation of the experiment in Table 1 line ii; the components and overall motion of virtual gauge arrays at 0.4 and 8.4 mm depth are shown with the Z-axis representing the impact axis and intended vector of one-dimensional motion (see Figure 5). The components of off-impact axis motion seen in the simulation were minimal, on the order of less than 0.1% of the impact axis motion. While not accounting for the physical presence of gauge elements themselves, this implies that while there is a potential for error due to the generation of a pesuedo one-dimensional wavefront as the graded areal density elements of the flyers employed here collapse, that it is not significant when compared to other sources of experimental error such as tilt.

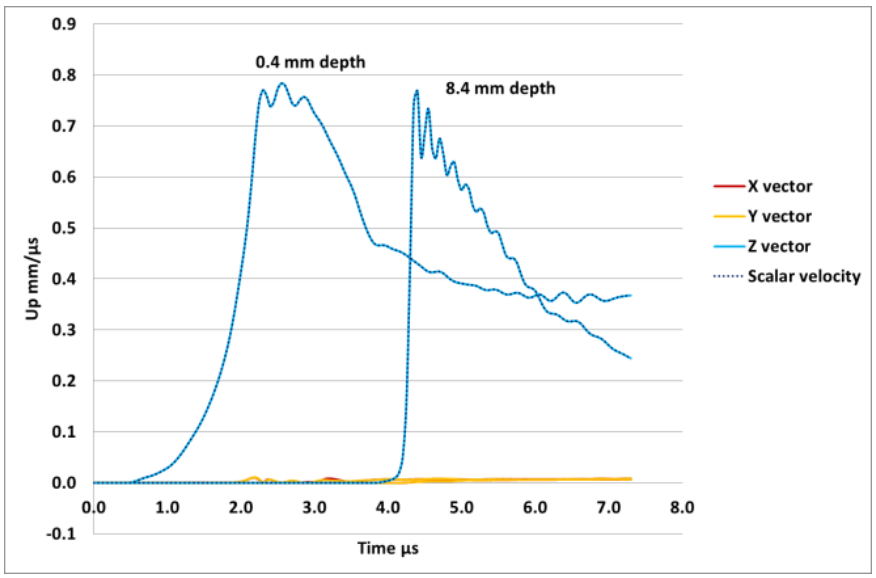

Figure 7: Graph showing components of motion observed in simulation of experiment detailed in Table 1 line ii. The components of motion observed by the virtual gauge array are minimal except in the intended axis of one dimensional motion (z-axis).

The other purpose of the simulations was to gain an insight into the mode of operation of the spike/buffer system. Figure 8 shows several snapshots from a simulated experiment. In these snapshots, the spikes can be seen to collapse and fail upon impact with the buffer. This produces multiple wavelets in the buffer which converge to form a pseudo one-dimensional wavefront in the target.

This results in a loading entering the target that has a two part structure. The initial ramp loading portion is controlled by the tips of the spikes, this is then followed by a shock dominated by the base of the flyer before release effects (from the rear edge of the base of the flyer) occur.

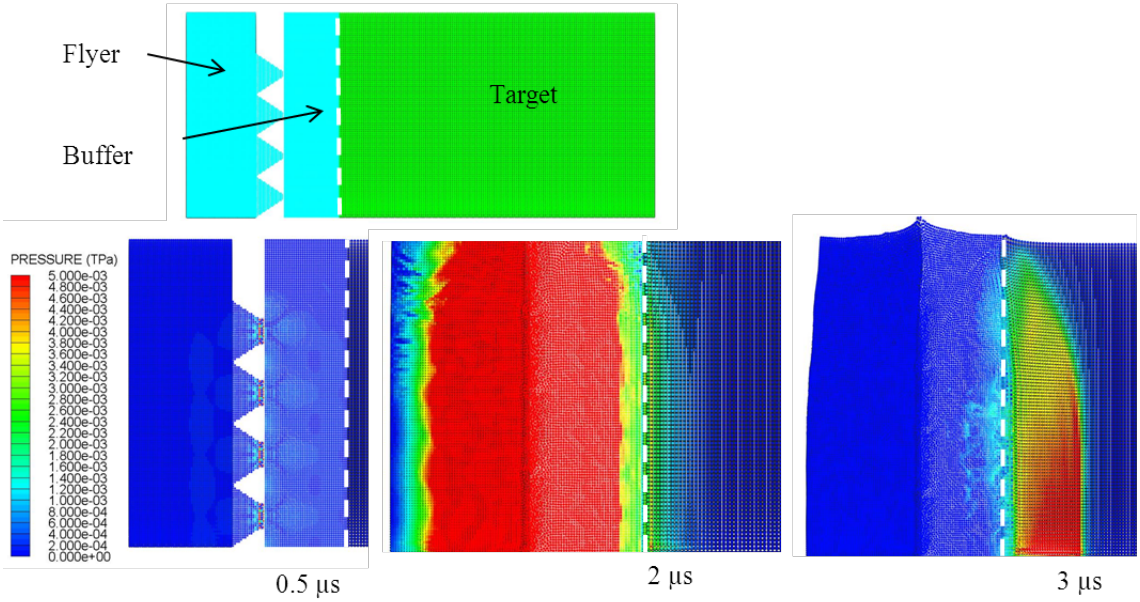

Figure 8: Snapshots taken from Autodyn™ simulation. The experiment represented is ii) in Table 1. Colours represent pressure contours and timings from start of simulation are shown. The interface between buffer and target is shown by the dashed white line.

5. Experimental Results

Experiments were carried out using two 50 mm smooth bore gas guns based at Cranfield University [26]. The embedded gauge used here was a design based that used at LANL [4,5] – although with a copper/polyimide construction. Magnetic fields were provided by two sets of NdFeB N50 permanent magnets, with field strengths of 195 ± 3.9 and 189.6 ± 0.3 mT respectively [10].

The gauges used each contained nine active elements and three shock trackers. A schematic of the gauge and target assembly is shown in Figure 9, along with a photo of the target mounted within the magnet array. The gauge is positioned in the target so that when motion occurs, the active elements of the gauge (the vertical elements labelled in Figure 9) produce a voltage. This is governed by Equation 1, and so the particle velocity of gauge (and therefore the surrounding material) can be calculated. In Equation 1, V is the voltage, B is the strength of the magnetic field, L is the length of the active element and U_p is the particle velocity.

$$V = BLU_p \tag{1}$$

Shock trackers consist of a closed loop containing a large number of closely spaced elements. As a shock traverses each element the polarity of the voltage produced changes from positive to negative, enabling high fidelity shock velocity measurements to be made. In this instance it was found that the shock trackers did not respond well to a ramp loading, with sharp polarity transitions not visible during the ramping portion of the loading. However, the shock

tracker data was still useful as ‘tilt pins’, showing how planar the ramp loading was across the gauge package.

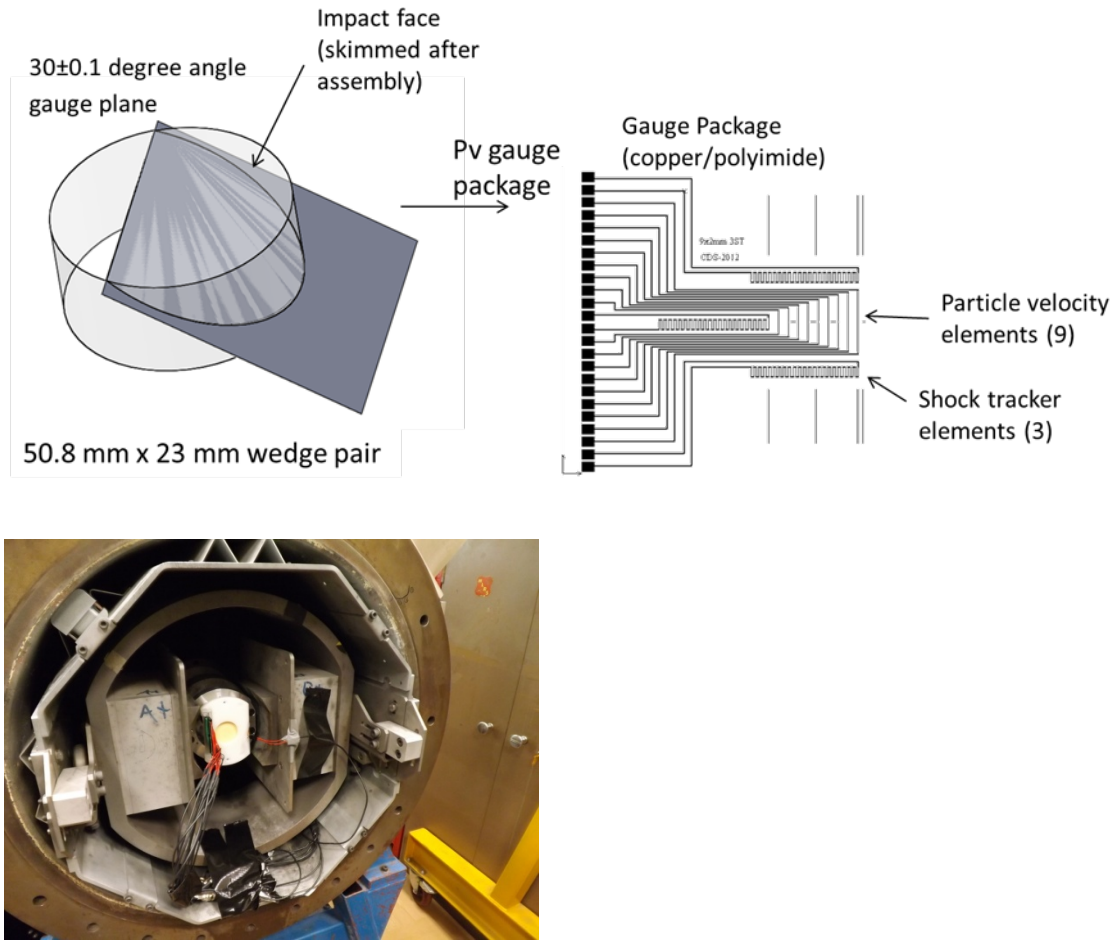

Figure 9: PV gauge and target assembly (top) and target mounted within NdFeB magnet array (field 189.6±0.3 mT) (bottom).

Key experimental results (in the form of interpreted particle velocity – time traces) are detailed in Figures 10 and 11i-viii. The particle velocity results are calculated from the

voltage induced in the gauge elements. Early experiments used a 5 mm thick rapid prototype ceramic buffer, while later experiments used a 4.2 mm thick Alotec 98 SB buffer of similar density. Note that only alternate traces are displayed for clarity.

By altering the values of parameters such as the spike height (A in Figure 1), the flyer designs are capable of producing a range of ramp loadings in the target material. A summary graph (Figure 10) shows varying ramps produced at two depths in a Kel-F target, the 10 mm spiked flyer is not represented here as it was not used for a high velocity impact. Figure 10 shows a comparison of 5 mm, 2 mm (several variations, see Table 1) and 1 mm spike height systems for a Kel-F target. As can be seen a wide variety of loadings can be produced; these can be further altered by varying the thickness of the buffer plate used. For the 1 and 2 mm systems it can seen that the loading has transitioned from an initial ramp to a steep shock by 8 mm depth, whereas for the 5 mm system this has not occurred. By optimization of the buffer thickness this transition can be controlled. Notably, the peak particle velocities seen for all systems are near identical within the expected variation caused by a slightly varying inter-shot impact velocity, although (as might be expected), shock velocities were found to vary by a greater extent.

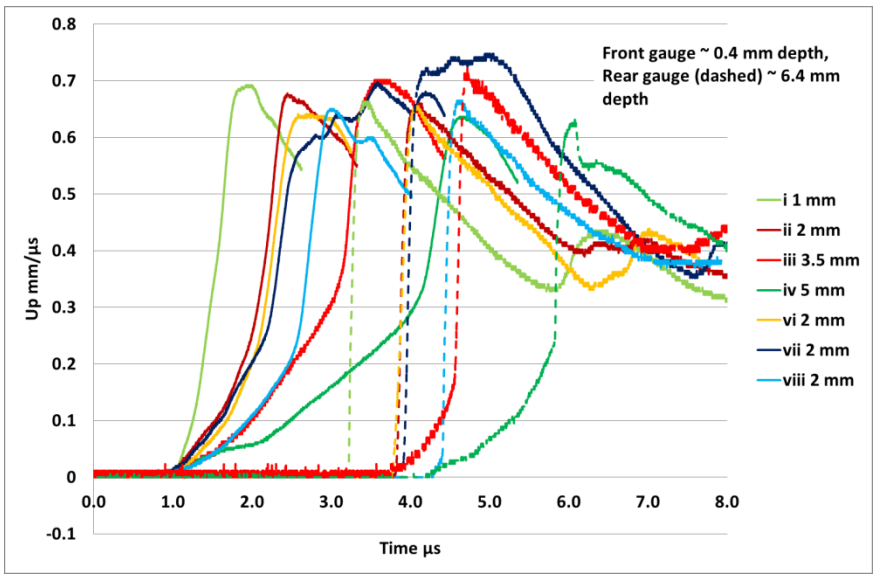

Figure 10: Comparison of selected experimental data for spike systems described in Table 1. Impacts were at a range of velocities consisting of 0.975 ± 0.025 mm/μs. Note that the traces here are truncated for clarity.

As discussed, Figure 11i-viii below shows selected results from individual experiments. Figure 11i shows results for the 1 mm spike height system impacting a Kel-F 81 target. A smooth ramp loading or compaction wave can be observed in the shallower gauges, transitioning to a conventional shock loading after 2.4 mm depth. Two distinct wave velocities are seen. The initial time of arrival at the shallower gauges manifests a wave of velocity 1.92 mm/μs, which is subsequently overtaken by a second loading (visible as a particle velocity gradient change) that displays features resembling a conventional shock front (rapid loading). This suggests that the initial loading is controlled by the spikes, which then transitions to a regime dominated by the effect of the solid base. Peak particle velocities are

broadly similar over the observed material and are ~80% of what would be expected for a plate impact using similar materials/velocities. It can be observed that release effects appear to preclude the formation of a sustained shock. The observed particle velocity is lower than the modelling results indicate and oscillations seen in the computer simulation are not present or are not observed in the PV gauge results.

In Figure 11ii (2 mm spike height system), the time required for the shock portion of the loading to become dominant is substantially increased, although the maximum particle velocity reached and the wave velocities are similar. In this case the 'two part' structure of the loading can again be clearly observed. The 3.5 mm spikes (Figure 12iii) continue this trend; although here the shock does not overtake the ramp loading over the gauged region of the target. This experiment also utilised a stirrup gauge between the buffer and target interface (the gauge trace at zero depth in figure 12iii) – with the increased particle velocity observed by the stirrup attributed to the impedance mis-match between the ceramic and polymer materials. The particle and shock velocities observed in the embedded gauge are slightly higher than for other experiments due to this shot occurring at the higher end of the quoted velocity range. Increasing the spike height to 5 mm (Figure 11iv) again elongates the rise times of the loading, although particle and shock velocities remain similar. In this case all the gauges observe a similar loading, showing that the loading is consistent throughout the material and that the shock doesn't overtake the ramp over the gauged material region. It is noticeable that the agreement with the modelled results is better for the shallower ramp loadings. The later introduction of release effects confirms that these are related to the spacing of the spikes tips and the back surface of the flyer disc. Figure 11v shows the results of the 10

mm spike height system; note the lower impact velocity of 0.53 mm/μs in this case. It is apparent that here all the gauges observe a similar particle velocity history, showing that the loading is consistent throughout the material and that again the shock does not overtake the ramp over the gauged material region. Essentially, the shock is not observed before release effects dominate.

Figures 11vi-viii show the results of several variations on the 2 mm spike height flyer. Reducing the side length of the base of the spikes (parameter B in Table 1) is shown in figure 11vi. This extends the period of the ramp phase of the loading and also increases the period of the pseudo-sustained shock loading (or plateau). This is an important effect as it enables easier comparison with conventional sustained shock experiments. Figure 11vii shows the result of introducing a thicker base to the flyer (parameter G in Table 1). This appears to delay the production of the shock portion of the loading, with the particle velocity within the target taking longer to reach a maximum particle velocity. The release effects seen are similarly delayed. It is possible that alteration of the buffer thickness is required in this case to optimise the loading observed so that peak particle velocity is reached nearer the surface of the target. Lastly, Figure 11viii shows the result of introducing a spacing between the spikes (parameter D in Table 1), in effect reducing the packing density. This has a surprisingly limited effect on the loading observed and actually improves the planarity of the plateau of the loading observed at the shallower gauges.

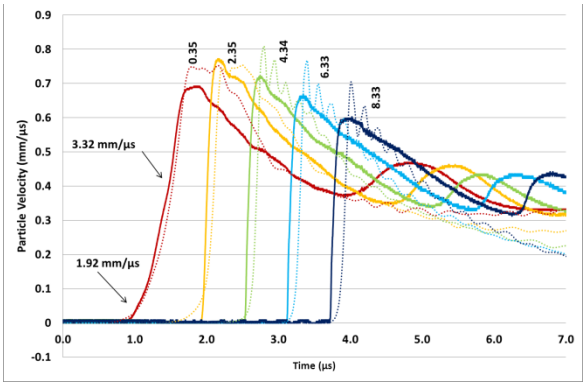

i) 1 mm spike height

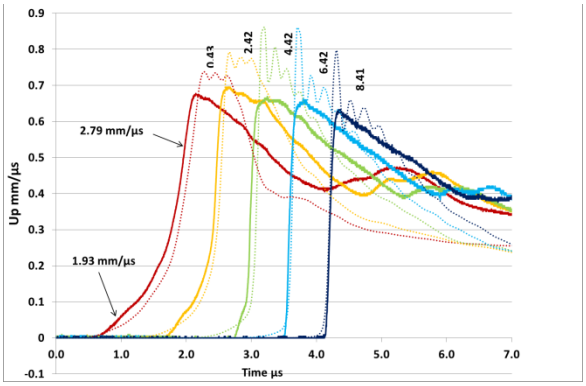

ii) 2 mm spike height

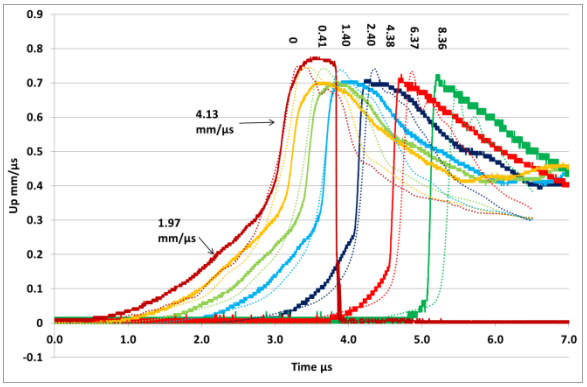

iii) 3.5 mm spike height (0 indicates the stirrup gauge)

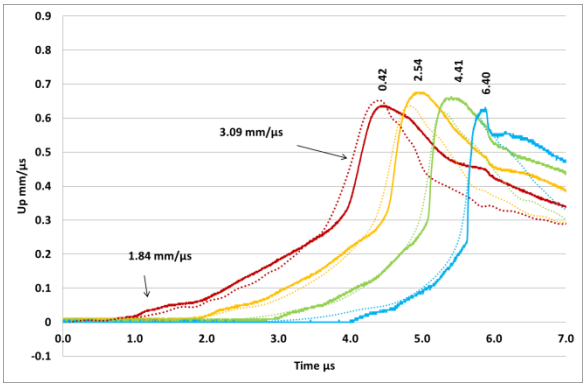

iv) 5 mm spike height

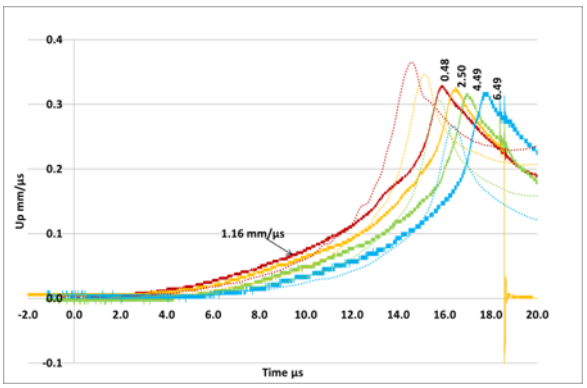

v) 10 mm spike height

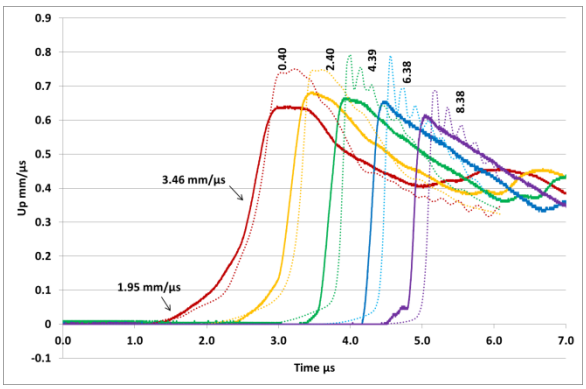

vi) 2 mm spike height (2 mm base side)

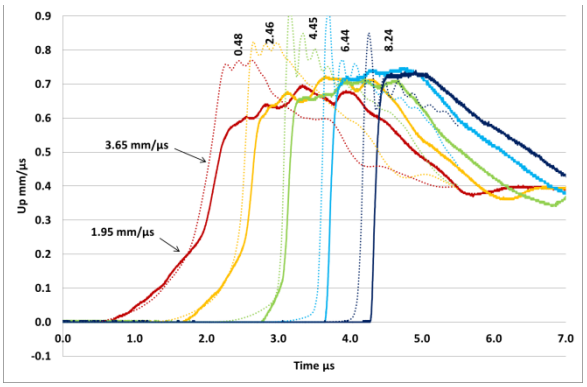

vii) 2 mm spike height (10 mm thick base)

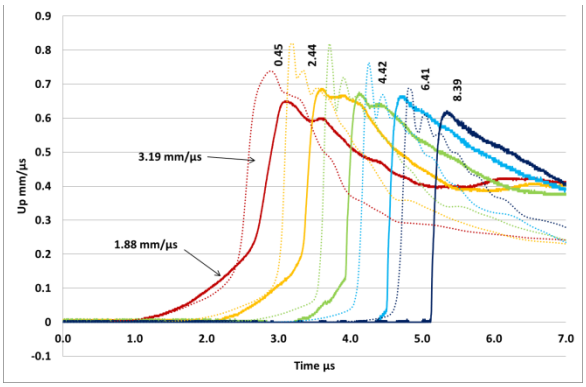

viii) 2 mm spike height (reduced packing density)

Figure 11: Comparison of selected experimental (solid) and modelling (dotted) data for various spike height flyer systems; trace labels indicate the distance of the gauge element relative to the target/buffer interface (mm). Wave velocities of ramp and shock portions of loading are indicated. Impact velocity was 0.975 ± 0.025 mm/μs apart from E), where impact velocity was 0.53 mm/μs. Labels A-H correspond to similar labels in Table 1.

6. Discussion

The experimental results appear to indicate that upon impact the spikes form multiple wavelets in the buffer plate, which then coalesce and constructively interfere, forming a quasi one-dimensional wavefront which then enters the target. The target then undergoes a complex loading path which can best be described as a ramp loading which comprises features of both shockless compression and a shockwave. In the designs tested so far, an initial ramping wave controlled by the tips of the spikes enters the target and is then subsequently overtaken by a shock dominated by the solid ceramic base. A development objective is to optimise the flyer and buffer parameters to form a period of sustained shock in the targets. It is likely that this will involve undertaking an iterative set of simulations which in turn would necessitate carrying out a full characterisation of the rapid prototyped ceramic. Quantifying the exact mechanism of spike collapse is the subject of continuing hydrocode modelling work.

In general good agreement can be seen between experimental and modelling results, although the simulations do exhibit several deviations from the experimental results. There are two main discrepancies. Firstly the simulations produce a ~ 10% higher particle velocity then that seen in the experimental results. This is likely due to inaccuracies in the EOS used to represent the ceramic components. As previously mentioned a standard Autodyn™ library model for Al 99.7 ceramic [22] was used to represent both the flyers and buffers. From results of reverse ballistics experiments (not presented here), the authors believe it likely that the rapid prototyped ceramic is weaker in tension than conventionally pressed material of a similar density. This is possibly due to the (proprietary) manufacturing process requiring that the material is only sintered under heat, rather than both heat and pressure as-per a

conventional ballistic grade ceramic. Additionally, on a related front, it was noted that several thick (10 and 20-mm thick) discs of the material supplied for characterisation had thin cracks in them along the z-axis – i.e. the axis in which layers are solidified during the build process. This style of defect only seemed to occur with discs > 5-mm thick. Although the flyer discs underwent electron microscopy and Micro-CT examination without discovery of such defects, weaknesses could still be present. The other main discrepancy is the oscillations seen in the simulated particle velocity traces. These were found to be an artefact of the particle size used in the simulation. The current particle size used in the simulations was shown to offer a balance between reducing the oscillations and making efficient use of computational resources.

One limit of the technique currently employed is the combination of alumina ceramic material and the maximum achievable launcher velocity, issues which necessarily impose a limit on the magnitude of the loadings that can be produced. On this front, rapid prototyped zirconia ceramic (currently under development at Technology Assessment and Transfer [20]), would enable higher shock pressures to be generated in targets and give more scope for alternation of ramp parameters.

7. Conclusions

The graded areal density flyer technique has been successfully applied to polymeric targets using rapid prototyped alumina ceramic. Quasi one-dimensional loadings which progress from shockless compression to a shock wave have been observed in Kel-F targets using embedded particle velocity gauges. This methodology provides a viable and novel way of generating ramp wave loading in materials, particularly in cases where the use of metallic flyer materials is not viable.

Further, hydrocode modelling has produced simulations which qualitatively predict the failure mechanisms of the spikes and the loading that is induced in the target. Reasonable agreement with experimental results has been achieved using a standard alumina ceramic equation of state. This agreement is expected to improve once the intricacies of the rapid prototyped ceramic material are fully characterised, thus providing the opportunity to tailor this novel approach further in future.

Acknowledgements

This work was carried out in support of an ISP (Imperial College, London, UK) funded PhD.

The authors would like to thank Andrew Roberts (Cranfield University, UK) for technical assistance.

References

[1] Goff M, Burns M J, Stennett C, Roberts A, Appleby-Thomas G J 2014 Ramp loading of Kel-F 81 and EDC 37 observed with embedded particle velocity gauges, *Submitted to 15th Int. Det. Symp.,* 2014

[2] Taylor P, Goff M, Hazell P, Leighs J, Wood D, Appleby-Thomas G J 2014 Ramp wave generation using graded areal density ceramic flyers and the plate impact technique *J. Phys.: Conf. Ser.* Vol. 500

[3] Field J E, Walley S M, Proud W G, Goldrein, H T, Siviour C R Review of experimental techniques for high rate deformation and shock studies. *Int J Impact Eng*. 30:725–75

[4] Sheffield S A, Gustavsen R L and Alcon R R 1999 In-situ magnetic gauging technique used at LANL -method and shock information obtained, *AIP Conf Proc*, **505** 1043

[5] Stennett C, Cooper G A, Hazell P J and Appleby-Thomas G 2009 Initiation of secondary explosives measured using embedded electromagnetic gauges *AIP Conf. Proc*. **1195** 267

[6] Orlikowski D, Nguyen J H, Patterson J R, Minch R, Martin L P and Holmes N C 2007 New experimental capabilities and theoretical insights of high pressure compression waves *AIP Conf. Proc*. **955** 1186

[7] Barker L M 1984 High-pressure quasi-isentropic impact experiments *Shock Waves in Condensed Matter* Elsevier Science Publishers B.V. 217

[8] Goff M, Burns M, Gustavsen R, Stennett C, Hazell P, Appleby-Thomas G J 2014 Effects observed when using metallic flyers and barriers with the embedded particle velocity gauge technique *J. Phys.: Conf. Ser.* Vol. 500

[9] Winter R E, Cotton M, Harris E J, Chapman D J and Eakins D 2014 A novel graded density impactor *J. Phys.: Conf. Ser.* Vol. 500

[10] Burns M J, Routley N R and Hazell P J 2011 A novel technique to study build up to detonation from an attenuating shockwave in 1D explosive experiments, *Proceedings of the 42nd International Annual Conference of the Fraunhofer ICT*, 41

[11] Burns M J, Goff M, Stennett C, Roberts A 2014 Project Magnes – a Permanent Magnet Array for the Particle Velocity Gauge Diagnostic, *Submitted to 15th Int. Det. Symp*

[12] Lyzenga G A, and Thomas J A 1982 One-dimensional isentropic compression, *Shock Waves in Condensed Matter-1981*, vol. 78, no. 1, pp. 231-235

[13] Qiang S, Zhang L, Xiong H, Hua J, and Tan H 2000 Fabrication of W-Mo-Ti system flier-plate with graded impedance for generating quasi-isentropic compression, *Chinese Science Bulletin* 45, no. 15: 1421-1424

[14] Martin L P, Orlikowski D, and Nguyen J H 2006 Fabrication and characterization of graded impedance impactors for gas gun experiments from tape cast metal powders, *Materials Science and Engineering: A* 427, no. 1 (2006): 83-91.

[15] Setchell R E 1981 Ramp-wave initiation of granular explosives, *Combustion and Flame* 43:255-264.

[16] Bourne N K, Rosenberg Z, Ginzburg A 1996 The ramping of shock waves in three glasses. *Proc R Soc Math Phys Eng Sci*.452(1949):1491–6

[17] Baer M, Hall C, Gustavsen R, Hooks D, Sheffield S 2007 Isentropic loading experiments of a plastic bonded explosive and constituents. *J Appl Phys*. 2007;101(3):034906.

[18] Shen Z, Johnsson M, Zhao Z, Nygren M 2002 Spark Plasma Sintering of Alumina. *J Am Ceram Soc*. 2002;85(8):1921–7

[19] Travitzky, N, Bonet A, Dermeik B, Fey T, Filbert-Demut I, Schlier L, and Greil P 2014, Additive Manufacturing of Ceramic-Based Materials, *Advanced Engineering Materials*.

[20] Toll Ceramic Stereolithography, 2014 Private Communication, Technology Assessment & Transfer Inc, MD, USA

[21] SPH User Manual & Tutorial: Revision 4.3.2005 AUTODYN™ . Century Dynamics

[22] Westerling L and Lundberg T 1995 The Influence of Confinement on the Protective Capability of Ceramic Armour at Two Different Velocities *15th Int. Symp. on Ballistics* **1** 283 (Retrieved from Autodyn™ V14 material library)

[23] Johnson G R and Holmquist T J 1992 A computational constitutive model for brittle materials subjected to large strains, high strain rates and high pressures, *Shock Wave and High Strain Rate Phenomena in Materials* Marcel Dekker Inc. 1075

[24] Steinberg D J 1996 Equation of State and Strength Properties of Selected Materials, Technical Report URCL-MA-106439 Lawrence Livermore National Laboratory

[25] Arkema Group VOLTALEF® 300 HD PCTFE, retrieved February 2014 from http://www.matweb.com/search/DataSheet.aspx?MatGUID=7db2fe0407924045af967c3f10aa410b, Copyright 1996-2013 by MatWeb, LLC

[26] Bourne N K 2003 A 50 mm bore gas gun for dynamic loading of materials and structures. *Meas Sci Technol*. 14(3):273–8